

## Photocurrent induced by conducting channels of hole transporting layer to adjacent photoactive perovskite sensitized TiO<sub>2</sub> thin film: Solar cell paradigm

Sadia Ameen, M. Shaheer Akhtar, Hyung-Kee Seo, and Hyung-Shik Shin

*Langmuir*, Just Accepted Manuscript • DOI: 10.1021/la502398x • Publication Date (Web): 08 Oct 2014

Downloaded from <http://pubs.acs.org> on October 16, 2014

### Just Accepted

"Just Accepted" manuscripts have been peer-reviewed and accepted for publication. They are posted online prior to technical editing, formatting for publication and author proofing. The American Chemical Society provides "Just Accepted" as a free service to the research community to expedite the dissemination of scientific material as soon as possible after acceptance. "Just Accepted" manuscripts appear in full in PDF format accompanied by an HTML abstract. "Just Accepted" manuscripts have been fully peer reviewed, but should not be considered the official version of record. They are accessible to all readers and citable by the Digital Object Identifier (DOI®). "Just Accepted" is an optional service offered to authors. Therefore, the "Just Accepted" Web site may not include all articles that will be published in the journal. After a manuscript is technically edited and formatted, it will be removed from the "Just Accepted" Web site and published as an ASAP article. Note that technical editing may introduce minor changes to the manuscript text and/or graphics which could affect content, and all legal disclaimers and ethical guidelines that apply to the journal pertain. ACS cannot be held responsible for errors or consequences arising from the use of information contained in these "Just Accepted" manuscripts.



ACS Publications

High quality. High impact.

Langmuir is published by the American Chemical Society. 1155 Sixteenth Street N.W., Washington, DC 20036

Published by American Chemical Society. Copyright © American Chemical Society. However, no copyright claim is made to original U.S. Government works, or works produced by employees of any Commonwealth realm Crown government in the course of their duties.

1  
2  
3     **Photocurrent induced by conducting channels of hole transporting layer to adjacent**  
4         **photoactive perovskite sensitized TiO<sub>2</sub> thin film: Solar cell paradigm**

5     **Sadia Ameen<sup>†a</sup>, M. Shaheer Akhtar<sup>†b</sup>, Hyung-Kee Seo<sup>a\*\*</sup> and Hyung-Shik Shin<sup>\*a</sup>**

6             <sup>a</sup>Energy Materials & Surface Science Laboratory, Solar Energy Research Center, School of  
7             Chemical Engineering, Chonbuk National University, Jeonju, 561-756, Republic of Korea

8             <sup>b</sup>New & Renewable Energy Material Development Center (NewREC), Chonbuk National  
9             University, Jeonbuk, Republic of Korea

---

10     **Abstract**

11         The high performance perovskite solar cell was fabricated using distinguished  
12         morphology of polyaniline nanoparticles (PANI-NPs) as efficient hole transporting layer (HTL)  
13         with methyl ammonium lead iodide perovskite ( $\text{CH}_3\text{NH}_3\text{PbI}_3$ ) as sensitizer. PANI NPs were  
14         simply synthesized by the oxidative chemical polymerization of aniline monomer at 0-5 °C. The  
15         reasonable solar-to-electricity conversion efficiency of ~6.29 % with high short circuit current  
16         ( $J_{\text{SC}}$ ) of ~17.97 mA/cm<sup>2</sup> and open circuit voltage ( $V_{\text{OC}}$ ) of ~0.877 V were accomplished by  
17         Ag/PANI-NPs/ $\text{CH}_3\text{NH}_3\text{PbI}_3$ /mp-anatase-TiO<sub>2</sub>/bl-TiO<sub>2</sub>/FTO perovskite solar cell. The transient  
18         photocurrent and photovoltage studies revealed that the fabricated solar cell showed better  
19         charge transport time, diffusion coefficient, diffusion length and the charge collection efficiency.  
20         Herein, the use of PANI NPs as HTL improved the charge carrier generation and the charge  
21         collection efficiency of the fabricated solar cell.

22  
23  
24  
25  
26  
27  
28  
29  
30     **Keywords:** Polyaniline, nanoparticles, perovskite, thin film, solar cells, charge collection  
31         efficiency

32         \*Corresponding author. Tel: +82-63-270-2438, Fax: +82-63-270-2306

33         E-mail address: [hsshin@jbnu.ac.kr](mailto:hsshin@jbnu.ac.kr) (H. S. Shin), \*\*[enterprise2@jbnu.ac.kr](mailto:enterprise2@jbnu.ac.kr) (H. K. Seo)

34         †Authors contributed equally to this work

## 1. INTRODUCTION

A new kind of inorganic-organic solar cell based on organic halide perovskite materials have recently gained a great deal of attention due to good electron and hole conductivity,<sup>1-3</sup> high carrier mobility ( $50 \text{ cm}^2/\text{V.s}$ ),<sup>4</sup> direct band gap ( $\sim 1.55 \text{ eV}$ ) and high stability.<sup>5</sup> Interestingly, the perovskite as sensitizer displays a very strong absorption in the visible region to the near infrared region<sup>6,7</sup> and their optical and electronic properties could be tuned by changing the chemical compositions of perovskites.<sup>2,8</sup> The light absorption in perovskites solar cell could be improved by using light absorbing polymers as HTLs, which could improve the optical density of the mesoporous thin films due to the advancement in the light harvesting by the hole-conductors with the pores of thin films.<sup>9,10</sup> The perovskites are highly versatile materials with spectral tunability which efficiently improves the photoinduced electron transfer from the p-type polymers to n-type metal oxides thin films.<sup>11,12</sup>

In general, the hole transporting material, 2,2',7,7'-tetrakis-(N,N-di-p-methoxyphenyl-amine)- 9,9'-spirobifluorene (spiro-MeOTAD) is commonly used in various dye sensitized solar cells and perovskite solar cells because it shows the efficient charge transport, low recombination rates and improves the pore filling of  $\text{TiO}_2$  layer. Hitherto, the synthetic process of spiro-MeOTAD is excessively costly at the laboratory level and therefore, it is important to find cheap and effective alternatives to spiro-MeOTAD for the fabrication of low cost perovskite solar cells. So far, several conducting polymers such as poly-[2,1,3-benzothiadiazole-4,7-diyl [4,4-bis(2-ethylhexyl)-4H-cyclopenta [2,1-b:3,4-b'] dithiophene-2,6-diyl]] (PCPDTBT), (poly-[[9-(1-octynonyl)-9H-carbazole-2,7-diyl]-2,5-thiophenediyl-2,1,3-benzothiadiazole-4,7-diyl-2,5-thiophenediyl]) (PCDTBT) and poly-triarylamine (PTAA) have been used as HTLs or electron-

1  
2  
3 blocking layers for the fabrication of perovskite solar cells.<sup>13</sup> A apart from various conducting  
4 polymers, polyaniline (PANI) is one of the most extensively studied polymers owing to its ease  
5 of synthesis, high conductivity, and the good environmental stability.<sup>14</sup> PANI shows versatility in  
6 nanostructures of nanofibers, nanorods, nanowires, nanotubes and nanoflakes with high surface  
7 to volume ratio and low diffusional resistance.<sup>15</sup> PANI nanomaterials are widely used for the  
8 fabrication of efficient electronic and nanodevices such as FETs, sensors, catalysis, photovoltaics  
9 etc. due to its improved optical, structural, electronic and electrical properties.<sup>16</sup> Recently, Y.  
10 Xiao et al. fabricated the solid-state perovskite-sensitized solar cell using dual function of PANI  
11 with brachyplast structure, in which PANI structure was deposited by a two-step cyclic  
12 voltammetry (CV) approach.<sup>17</sup> Inspired by the aforementioned development, a highly efficient  
13 solar cell is fabricated using organic halide perovskite ( $\text{CH}_3\text{NH}_3\text{PbI}_3$ ) as light harvester which is  
14 coated on mesoporous  $\text{TiO}_2$  and the organic PANI NPs is applied as HTL. In this work, the  
15 fabricated perovskite solar cell achieves reasonably high incident-photon-to-current efficiency  
16 (IPCE) of ~51% in the wavelength range of ~450-700 nm and maximum overall solar-to-  
17 electricity conversion efficiency of ~6.29 % under AM 1.5 illumination at an intensity of 100  
18 mW cm<sup>-2</sup>. The use of PANI NPs as HTL has substantially improved the charge carrier generation  
19 and the charge collection efficiency of the fabricated perovskites solar cell.

## 2. EXPERIMENTAL

### 2.1 Synthesis of PANI NPs by oxidative chemical polymerization

In a typical synthesis of PANI NPs, 3 mmol of aniline monomer (0.27 ml, Sigma-Aldrich,  
≥99.5%) was dissolved in 10 ml DI (deionized) water under constant stirring at the room  
temperature. Thereafter, a separate solution of 10.9 mmol ammonium per-oxydisulphate (APS,

1  
2  
3 2.5g, Riedel-de-Haen, 97%) was prepared and added drop by drop into the prepared aniline  
4 monomer solution using peristaltic pump. Finally, the reaction mixture was kept for 12 h under  
5 static condition at 0-5 °C. The obtained greenish precipitates were centrifuged at ~4500 rpm for  
6 10 min and the desired product was washed with copious amount of DI water, methanol and  
7 dried in vacuum oven at 40 °C. In order to achieve the optimized condition for PANI NPs, the  
8 concentrations of aniline monomer were varied from 1 mmol - 6 mmol while the concentration  
9 of ammonium per-oxydisulphate was kept constant to 10.9 mmol, as presented in the supporting  
10 information.  
11  
12  
13  
14  
15  
16  
17  
18  
19  
20  
21  
22  
23  
24

## 2.2 Preparation of perovskite $\text{CH}_3\text{NH}_3\text{PbI}_3$ solution

25 The methyl ammonium iodide ( $\text{CH}_3\text{NH}_3\text{I}$ ) was synthesized as reported elsewhere.<sup>18</sup> In  
26 brief, the reactant mixture of methylamine (27.86 ml,  $\text{CH}_3\text{NH}_2$ , 40% in methanol, TCI  
27 chemicals) and hydroiodic acid (30 ml of 57 wt% in water, HI, Aldrich, 99%) were taken in 200  
28 ml round bottom flask. The reaction mixture was continuously stirred at 0 °C for 4 h and  
29 afterwards, the precipitates were recovered by the evaporation at 50 °C for 1 h. The obtained  
30 yellow product of  $\text{CH}_3\text{NH}_3\text{I}$  was repeatedly washed with diethyl ether (( $\text{C}_2\text{H}_5\text{O}_2$ )<sub>2</sub>O Alfa Aesar,  
31 99+% assay) and dried at 60 °C in vacuum oven for 24 h. The synthesis of  $\text{CH}_3\text{NH}_3\text{PbI}_3$  was  
32 carried out by mixing equimolar precursor solutions of  $\text{CH}_3\text{NH}_3\text{I}$  and lead iodide ( $\text{PbI}_2$ , Aldrich,  
33 99%) in γ-butyrolactone ( $\text{C}_4\text{H}_6\text{O}_2$ , TCI, 99%) at 60 °C for 12 h.  
34  
35  
36  
37  
38  
39  
40  
41  
42  
43  
44  
45  
46  
47  
48  
49  
50  
51  
52  
53  
54  
55  
56  
57  
58  
59  
60

## 2.3 Fabrication of perovskite solar cell (Ag/PANI-NPs/ $\text{CH}_3\text{NH}_3\text{PbI}_3$ /mp-anatase-TiO<sub>2</sub>/bl-TiO<sub>2</sub>/FTO)

The fluorinated tin oxide glass (FTO glass, Hartford Glass Co.,  $8\Omega/\text{sq}$ , 80% transmittance in visible spectrum) substrates were partially etched by using zinc powder (Aldrich, 99%) and 2M hydrochloric acid (HCl, Samchun Chemicals, 35-37%). The etched FTO substrates were cleaned by the ultrasonic bath using acetone, isopropanol and DI water. Thereafter, the etched FTO substrates were coated with blocking layer (bl) using 0.1 M Ti(IV) bis(ethyl acetoacetato)-diisopropoxide ( $\text{CH}_3\text{CH}_2\text{OCOCH}=\text{C(O-)}\text{CH}_3)_2\text{Ti}(\text{OCH}(\text{CH}_3)_2)_2$ , Alfa Aesar, 75% in Isopropanol) in 1-butanol ( $\text{C}_4\text{H}_9\text{OH}$ , Showa Chemicals, 99%) solution by spin-coating method and then the substrates were heated at  $500^\circ\text{C}$  for 30 min. The mesoporous (mp) anatase- $\text{TiO}_2$  layer was screen-printed on the pre-treated FTO glass substrates using diluted  $\text{TiO}_2$  paste (Solaronix) and again sintered at  $500^\circ\text{C}$  for 30 min. The synthesized perovskite solution was coated on the annealed  $\text{TiO}_2$  thin film through spin coating at the speed of  $\sim 2000$  rpm for 40 s using  $0.45\ \mu\text{m}$  pore PVDF membrane syringe filter (Jet Biofil) at ambient atmosphere. Thereafter, the thin films were annealed at  $100^\circ\text{C}$  for 30 min to achieve the  $\text{CH}_3\text{NH}_3\text{PbI}_3/\text{mp-anatase-TiO}_2/\text{bl-TiO}_2/\text{FTO}$ . PANI-NPs as HTL was spin-coated on  $\text{CH}_3\text{NH}_3\text{PbI}_3/\text{mp-anatase-TiO}_2/\text{bl-TiO}_2/\text{FTO}$  substrate at  $\sim 3000$  rpm for 30s using PANI solution in choloroform (15 mg/1 ml) with  $13.6\ \mu\text{l}$  Li-bis (trifluoromethanesulfonyl) imide ( $\text{CF}_3\text{SO}_2\text{NLiSO}_2\text{CF}_3$ , Li-TFSI)/acetonitrile (28.3 mg/1 ml, TCI, >98%) and  $\sim 6.8\ \mu\text{l}$  TBP ( $\text{C}_9\text{H}_{13}\text{N}$ , Aldrich, 96%) as additives in the ambient condition and dried at  $100^\circ\text{C}$  for 15 min to obtain PANI-NPs/ $\text{CH}_3\text{NH}_3\text{PbI}_3/\text{mp-anatase-TiO}_2/\text{bl-TiO}_2/\text{FTO}$ . Finally, Ag contact (thickness  $\sim 100$  nm) was made by the thermal evaporation to achieve Ag/PANI-NPs/ $\text{CH}_3\text{NH}_3\text{PbI}_3/\text{mp-anatase-TiO}_2/\text{bl-TiO}_2/\text{FTO}$  as fabricated perovskite solar cell.

## 2.4 Characterizations

The field emission scanning electron microscopy (FESEM, Hitachi S-4700) and the atomic force spectroscopy (AFM, Nanoscope IV, Digital Instruments, Santa Barbara, USA) were used to investigate the morphology of mp-anatase-TiO<sub>2</sub>/bl-TiO<sub>2</sub>/FTO, CH<sub>3</sub>NH<sub>3</sub>PbI<sub>3</sub>/mp-anatase-TiO<sub>2</sub>/bl-TiO<sub>2</sub>/FTO and Ag/PANI-NPs/CH<sub>3</sub>NH<sub>3</sub>PbI<sub>3</sub>/mp-anatase-TiO<sub>2</sub>/bl-TiO<sub>2</sub>/FTO thin films. The line scan element mapping was analyzed by the FESEM coupled Energy dispersive X-ray spectroscopy with the mapping mode. The crystalline nature and phases of CH<sub>3</sub>NH<sub>3</sub>PbI<sub>3</sub>/FTO and CH<sub>3</sub>NH<sub>3</sub>PbI<sub>3</sub>/mp-anatase-TiO<sub>2</sub>/bl-TiO<sub>2</sub>/FTO thin films were studied by X-ray powder diffraction (XRD, Rigaku, Cu K $\alpha$ ,  $\lambda = 1.54178\text{ \AA}$ ) in the Bragg angle ranging between 20°-80°. The optical properties of the deposited thin film were demonstrated by UV-Vis spectrophotometer (JASCO, V-670, Japan) and photoluminescence (PL) spectroscopy (JASCO, FP-6500). The current density (J)-voltage (V) measurements were performed for elucidating the performance of Ag/PANI-NPs/CH<sub>3</sub>NH<sub>3</sub>PbI<sub>3</sub>/mp-anatase-TiO<sub>2</sub>/bl-TiO<sub>2</sub>/FTO perovskite solar cell by using computerized digital multimeter (model 2000, Keithley) with a variable load under one sun (1.5 AM at 100 mW/cm<sup>2</sup>). A 1000 W metal halide lamp supplied the light and the intensity was adjusted to simulate 1.5 AM at 100 mW/cm<sup>2</sup> using a Si photo detector fitted with a Kα-5 filter as a reference, which was calibrated at NREL, USA. Before J-V measurements, a mask of black tape was pasted on top of the cell exempting the active area. The operating temperature was maintained in the range of 20-30 °C by a small cooling fan. The incident photon-to-current conversion efficiency (IPCE) was carried out by specially designed IPCE system for solar cell by PV measurements, Inc., USA. Before performing the IPCE measurements, the system was calibrated with a silicon photodiode, which was calibrated using the NIST-calibrated photodiode G425 as standard. The IPCE results of Ag/PANI/CH<sub>3</sub>NH<sub>3</sub>PbI<sub>3</sub>/mp-anatase-TiO<sub>2</sub>/bl-TiO<sub>2</sub>/FTO perovskite solar cell were collected as a function of wavelength from ~400-800 nm using 75 W

Xe lamp as a light source for generating monochromatic beam at a low chopping frequency. The charge collection efficiency and photoelectron density were revealed by the analysis using intensity-modulated photocurrent spectroscopy (IMPS) and intensity-modulated photovoltage spectroscopy (IMVS) using IVIUM technologies (CompactStat.e20250, USA).

### 3. RESULTS AND DISCUSSION

The morphological investigations are examined by taking the surface-view and cross section FESEM images of the fabricated perovskite solar cell, as shown in Figure 1. The surface view (Figure 1(a)) of TiO<sub>2</sub> exhibits the uniformly distributed mesoporous thin film of TiO<sub>2</sub> nanoparticles. After the perovskite coating, the thin film possesses uniform grain structure of microscale size which is completely penetrated into the mesoporous TiO<sub>2</sub> thin film deposited on FTO substrate (Figure 1(b)). The cross-sectional FESEM image (Figure 1(c)) reveals the layered structure of perovskite solar cell. From Figure 1(c), the thickness of overall fabricated perovskite solar cell is estimated as ~1.5 μm, consisting of CH<sub>3</sub>NH<sub>3</sub>PbI<sub>3</sub>/mp-anatase-TiO<sub>2</sub>/bl-TiO<sub>2</sub> mesoporous layer (~600-700 nm) which is uniformly capped by PANI-NPs HTL. A thin Ag contact layer of ~100 nm could be clearly seen on top of the active layer of the fabricated perovskite solar cell.

Figure 2 shows the topographic and three dimensional (3D) AFM images of the synthesized PANI-NPs and PANI-NPs/CH<sub>3</sub>NH<sub>3</sub>PbI<sub>3</sub>/mp-anatase-TiO<sub>2</sub>/bl-TiO<sub>2</sub> thin films. Figure 2(a) displays spherical aggregated nanoparticles of PANI with the average size of ~20 nm. The well-mixed structure of perovskite and PANI-NPs is observed in Figure 2 (c), indicating the good penetration of PANI-NPs into the perovskite thin film. From 3D AFM images (Figure 2(b, d)), PANI-NPs/CH<sub>3</sub>NH<sub>3</sub>PbI<sub>3</sub>/mp-anatase-TiO<sub>2</sub>/bl-TiO<sub>2</sub> thin film shows the less rough surface

1  
2  
3 compared to PANI-NPs thin film. The root mean roughness ( $R_{rms}$ ) of films is calculated by the  
4 AFM images of the thin films. PANI-NPs thin film obtains the higher  $R_{rms}$  value (~46.5 nm) than  
5 PANI-NPs/ $\text{CH}_3\text{NH}_3\text{PbI}_3$ /mp-anatase-TiO<sub>2</sub>/bl-TiO<sub>2</sub> thin film (~28.2 nm), indicating the good pore  
6 filling of mesoporous TiO<sub>2</sub> thin film along with the perovskite sensitizer.  
7  
8  
9  
10  
11

12 The elemental compositions of each layer in PANI-NPs/ $\text{CH}_3\text{NH}_3\text{PbI}_3$ /mp-anatase-  
13 TiO<sub>2</sub>/bl-TiO<sub>2</sub> thin film are estimated by the elemental mapping and line scanning of cross-  
14 sectional view through electron X-rays dispersive spectroscopy (EDS), as depicted in Figure 3.  
15 The mapping image (Figure 3(a)) displays that the thin film is majorly comprised of C, Ti, O, N,  
16 I and Pb with atomic % of ~9.25%, ~28.76% ~56.26% ~3.74%, 0.51 and 1.48% respectively.  
17 The similar patterns are seen in the line scanning profile, as shown in Figure 3(b). It has been  
18 observed that the atomic % ratio of Pb to I is 1:3, which deduces the formation of PbI<sub>3</sub> in the  
19 perovskite sensitizer.  
20  
21

22 The X-ray diffraction patterns of  $\text{CH}_3\text{NH}_3\text{PbI}_3$ /mp-anatase-TiO<sub>2</sub>/bl-TiO<sub>2</sub>/FTO and  
23  $\text{CH}_3\text{NH}_3\text{PbI}_3$ /FTO thin films are examined to investigate the crystalline nature of the perovskite  
24 sensitizer deposited on TiO<sub>2</sub> thin film. Figure 4 (a) shows the diffraction peaks at ~14.2°, ~19.6°,  
25 ~28.6°, ~32.1°, ~40.6° and ~43.3°, which correspond to (110), (112), (220), (310), (224), and  
26 (314) crystal planes of the tetragonal perovskite structure.<sup>19,20</sup> Whereas, the other peaks at ~26.6°,  
27 ~33.8°, ~37.7, ~51.4°, and ~54.6° belong to the FTO layer of the glass substrate.<sup>16</sup> The XRD  
28 pattern of  $\text{CH}_3\text{NH}_3\text{PbI}_3$ /mp-anatase-TiO<sub>2</sub>/bl-TiO<sub>2</sub>/FTO exhibits the visible TiO<sub>2</sub> diffraction peaks  
29 along with significant perovskite and the FTO diffraction peaks. Importantly, no impurity peaks  
30 other than the deposited materials are observed, suggesting that  $\text{CH}_3\text{NH}_3\text{PbI}_3$ /mp-anatase-  
31 TiO<sub>2</sub>/bl-TiO<sub>2</sub>/FTO thin film possess pure phase of  $\text{CH}_3\text{NH}_3\text{PbI}_3$  and TiO<sub>2</sub> materials.  
32  
33  
34  
35  
36  
37  
38  
39  
40  
41  
42  
43  
44  
45  
46  
47  
48  
49  
50  
51  
52  
53  
54  
55  
56  
57  
58  
59  
60

The ultraviolet-visible (UV-vis) and the room temperature photoluminescence (PL) spectroscopy of  $\text{CH}_3\text{NH}_3\text{PbI}_3/\text{FTO}$  and PANI-NPs/ $\text{CH}_3\text{NH}_3\text{PbI}_3/\text{FTO}$  thin films are analyzed to investigate the optical properties. Figure 5(a) shows a typical UV-vis absorption spectrum of  $\text{CH}_3\text{NH}_3\text{PbI}_3/\text{FTO}$  thin film. From the derived tauc plot,  $\text{CH}_3\text{NH}_3\text{PbI}_3/\text{FTO}$  thin film exhibits the optical bandgap ( $E_g$ ) of  $\sim 1.69$  eV, which is consistent with the other reports of  $\text{CH}_3\text{NH}_3\text{PbI}_3$ .<sup>20,21</sup> The deposited  $\text{CH}_3\text{NH}_3\text{PbI}_3/\text{FTO}$  thin film absorbs a higher wavelength edge near  $\sim 700$  nm. However, after the deposition of PANI-NPs on  $\text{CH}_3\text{NH}_3\text{PbI}_3/\text{FTO}$  thin film, a red shift occurs and decreases the optical band gap. The increase in the peak intensity of UV-Vis spectra of PANI-NPs/ $\text{CH}_3\text{NH}_3\text{PbI}_3/\text{FTO}$  thin film might ascribe to the selective interactions between  $\text{CH}_3\text{NH}_3\text{PbI}_3$  and the quinoid ring of PANI-NPs, which might facilitate the charge transfer from quinoid unit to  $\text{CH}_3\text{NH}_3\text{PbI}_3$  via highly reactive imine groups. The room temperature PL spectra of  $\text{CH}_3\text{NH}_3\text{PbI}_3/\text{FTO}$  and PANI/ $\text{CH}_3\text{NH}_3\text{PbI}_3/\text{FTO}$  thin films are carried out with an excitation wavelength of  $\sim 320$  nm. Figure 5(b) shows that  $\text{CH}_3\text{NH}_3\text{PbI}_3/\text{FTO}$  and PANI-NPs/ $\text{CH}_3\text{NH}_3\text{PbI}_3/\text{FTO}$  thin films display similar emission bands in the blue and green regions. Noticeably, PANI-NPs/ $\text{CH}_3\text{NH}_3\text{PbI}_3/\text{FTO}$  thin film presents the lower PL intensity than  $\text{CH}_3\text{NH}_3\text{PbI}_3/\text{FTO}$  thin film due to the significant PL quenching which clearly indicates a contact between perovskite layer and PANI layer. The occurrence of PL quenching might facilitate the charge-carriers generation in  $\text{CH}_3\text{NH}_3\text{PbI}_3$  at PANI-NPs/ $\text{CH}_3\text{NH}_3\text{PbI}_3/\text{FTO}$  interface.<sup>22</sup>

A schematic representation of the fabricated perovskite solar cell is depicted in Figure 6(a). The first layer of the fabricated solar cell is formed by  $\text{TiO}_2$  blocking layer followed by the crystalline mesoporous (mp)  $\text{TiO}_2$  layer on the FTO substrate. The crystalline  $\text{CH}_3\text{NH}_3\text{PbI}_3$  are deposited on top of the mp-anatase- $\text{TiO}_2$  by the solvent-drying during spin-coating, followed by evaporation at  $80$  °C under vacuum. The hole transport layer (PANI-NPs) is coated on the

layered structure of the  $\text{CH}_3\text{NH}_3\text{PbI}_3/\text{mp-anatase-TiO}_2/\text{bl-TiO}_2$  thin film in which HTL assists in the hole extraction to the top deposited Ag electrode. Figure 6(b) shows the energy level diagram of perovskite solar cell. Under light illumination, the photons are absorbed by  $\text{CH}_3\text{NH}_3\text{PbI}_3$  and create the electron-hole pairs. Thereafter at the  $\text{CH}_3\text{NH}_3\text{PbI}_3/\text{mp-anatase-TiO}_2/\text{bl-TiO}_2$  interface, the generated excitons dissociate and the photoexcited electron injects into the conduction band of  $\text{TiO}_2$ , and simultaneously hole reaches to HTL. During the operation of solar cell, some of the remaining holes run across the perovskite layer before reaching to HTL. The exciton dissociates and the charge transfers at  $\text{CH}_3\text{NH}_3\text{PbI}_3/\text{mp-anatase-TiO}_2/\text{bl-TiO}_2$  and  $\text{PANI/CH}_3\text{NH}_3\text{PbI}_3/\text{mp-anatase-TiO}_2/\text{bl-TiO}_2$  interfaces to generate the energy. The bottom section of perovskite solar cell acts as an electron collector which is composed of ~100 nm thick hole-blocking compact  $\text{TiO}_2$  film deposited on the FTO followed by the deposition of ~600-700 nm thick layer of  $\text{PANI/CH}_3\text{NH}_3\text{PbI}_3/\text{mp-anatase-TiO}_2/\text{bl-TiO}_2$ .

The photovoltaic parameters of the fabricated  $\text{Ag/PANI-NPs/CH}_3\text{NH}_3\text{PbI}_3/\text{mp-anatase-TiO}_2/\text{bl-TiO}_2/\text{FTO}$  perovskites solar cell are obtained by measuring the current density-voltage (J-V) characteristics under a light intensity of  $100 \text{ mWcm}^{-2}$  (1.5 AM). The J-V curve is shown in the Figure 7(a) for the fabricated perovskite solar cells with and without PANI NPs. The overall solar-to-electric conversion efficiency of ~6.29 % with high short circuit current density ( $J_{SC}$ ) of ~ $17.97 \text{ mA.cm}^{-2}$ , open circuit voltage ( $V_{OC}$ ) of ~0.877 V and low fill factor (0.40) are accounted by the fabricated  $\text{Ag/PANI-NPs/CH}_3\text{NH}_3\text{PbI}_3/\text{mp-anatase-TiO}_2/\text{bl-TiO}_2/\text{FTO}$  perovskite solar cell. However, the inferior  $J_{SC}$  of ~ $9.67 \text{ mA/cm}^2$  and solar-to-electric conversion efficiency of ~1.95 % are observed for the fabricated solar cell without using PANI-NPs HTL, indicating that the introduction of PANI-NPs as HTL is a crucial step to improve the photovoltaic parameters. Importantly, the photocurrent and the photovoltage are much superior to dye-sensitized solar

1  
2  
3 cells based on PANI HTLs.<sup>23</sup> The uniform covering of HTL over CH<sub>3</sub>NH<sub>3</sub>PbI<sub>3</sub>/mp-anatase-  
4 TiO<sub>2</sub>/bl-TiO<sub>2</sub>/FTO thin film has reduced the recombination and the extraction of hole improves  
5 the charge transfer rate.<sup>24</sup> The small spherical nanoparticles of PANI might help to achieve the  
6 uniform surface coverage over CH<sub>3</sub>NH<sub>3</sub>PbI<sub>3</sub>/mp-anatase-TiO<sub>2</sub>/bl-TiO<sub>2</sub>/FTO thin film, which  
7 might reduce the occurrence of pin-holes (due to extraction of holes) and avoids the direct  
8 contact of HTL with mp-TiO<sub>2</sub> layer, and enhances the dark current leakages.<sup>4,25</sup> The performance  
9 of Ag/PANI-NPs/CH<sub>3</sub>NH<sub>3</sub>PbI<sub>3</sub>/mp-anatase-TiO<sub>2</sub>/bl-TiO<sub>2</sub>/FTO perovskite solar cell has been  
10 quantified on a macroscopic level in terms of the incidence photon to current conversion (IPCE)  
11 efficiency, as shown in Figure 7(b). The fabricated Ag/PANI-NPs/CH<sub>3</sub>NH<sub>3</sub>PbI<sub>3</sub>/mp-anatase-  
12 TiO<sub>2</sub>/bl-TiO<sub>2</sub>/FTO perovskite solar cell presents maximum IPCE value of ~51% in the  
13 wavelength range of ~450-700 nm and drops at longer wavelengths. The obtained IPCE is  
14 consistent with the J<sub>SC</sub> of the perovskite solar cells. Herein, PANI-NPs with high surface area  
15 might significantly improve the light scattering capacities and provides the better interaction  
16 between the photons and CH<sub>3</sub>NH<sub>3</sub>PbI<sub>3</sub> sensitizer. In order to investigate series and charge  
17 transfer resistances of the solar cells, the Nyquist plots are obtained from the fabricated  
18 perovskite solar cells with and without PANI-NPs under a frequency range from 100 kHz - 1 Hz,  
19 as shown in Figure 7. From impedance plots, the intercept of Z<sub>re</sub> at high frequency belongs to the  
20 ohmic series resistance (R<sub>S</sub>) and the diameter of first semicircle at high frequency represents the  
21 charge-transfer resistance (R<sub>CT</sub>) at PANI/CH<sub>3</sub>NH<sub>3</sub>PbI<sub>3</sub> interface.<sup>26</sup> The fabricated perovskite solar  
22 cells with and without PANI shows large R<sub>S</sub> values of ~20.5 Ω and ~41.2 Ω respectively. It is  
23 reported that the high R<sub>S</sub> effectively results to low fill factor and increases the recombination  
24 sites.<sup>27</sup> In our case, the fabricated perovskite solar cell with PANI obtains large R<sub>S</sub> which might  
25  
26  
27  
28  
29  
30  
31  
32  
33  
34  
35  
36  
37  
38  
39  
40  
41  
42  
43  
44  
45  
46  
47  
48  
49  
50  
51  
52  
53  
54  
55  
56  
57  
58  
59  
60

considerably result to low FF. However, the high  $J_{SC}$  is related to the improved transporting ability for the electron and hole, as observed the low  $R_{CT}$  values.

The intensity modulation photocurrent spectroscopy (IMPS) and the intensity modulation photovoltage spectroscopy (IMVS) measurements have been examined to elucidate the charge transfer and the recombination processes in the fabricated perovskite solar cells. IMPS and IMVS measurements are performed under the fixed light intensity at different voltages of light, as shown in Figure 8. From Figure 8, the charge-transport time ( $\tau_{CT}$ ) and the electron recombination time ( $\tau_R$ ) of the fabricated thin film solar cell are estimated using the minimum frequencies of IMPS and IMVS plots respectively.<sup>28</sup> The fabricated Ag/PANI-NPs/CH<sub>3</sub>NH<sub>3</sub>PbI<sub>3</sub>/mp-anatase-TiO<sub>2</sub>/bl-TiO<sub>2</sub>/FTO perovskite solar cell records the reasonable  $\tau_{CT}$  of ~25.2 ms and  $\tau_R$  of ~146 ms, suggesting the high charge transport rate and lesser recombination rate. Figure 9 (a,b) shows the plots of  $\tau_{CT}$  and  $\tau_R$  versus different photon flux of the fabricated perovskite solar cell which are derived by IMPS and IMVS. The order of  $\tau_{CT}$  and  $\tau_R$  value decreases with the increase of photon flux. The generation of electron-hole recombination and the electron diffusion in perovskite solar cell are examined by evaluating the electron diffusion length ( $D_L$ ) parameter i.e.  $D_L = (D_n \cdot \tau_R)^{1/2}$ ,<sup>29</sup> where  $D_n$  is diffusion coefficient obtained by IMPS plot. For the fabricated Ag/PANI-NPs/CH<sub>3</sub>NH<sub>3</sub>PbI<sub>3</sub>/mp-anatase-TiO<sub>2</sub>/bl-TiO<sub>2</sub>/FTO perovskite solar cell,  $D_n$  value is estimated as  $\sim 3.83 \times 10^{-6} \text{ cm}^2 \text{s}^{-1}$ . The relatively low  $D_L$  value of  $\sim 2.36 \mu\text{m}$  is observed by the fabricated perovskite solar cell which represents the probability of large electrons to enter from the CH<sub>3</sub>NH<sub>3</sub>PbI<sub>3</sub>/mp- anatase-TiO<sub>2</sub>/bl-TiO<sub>2</sub>/FTO thin film layers to the top Ag layer electrode. The low FF might result from the low  $D_L$  value. Moreover, the charge collection efficiency could be calculated by the relation  $\eta_{CC} = 1 - (\tau_{CT}/\tau_R)$  using  $\tau_{CT}$  and  $\tau_R$  values of the fabricated perovskite solar cell.<sup>29</sup> The high  $\eta_{CC}$  value is obtained

for the fabricated Ag/PANI-NPs/CH<sub>3</sub>NH<sub>3</sub>PbI<sub>3</sub>/mp-anatase-TiO<sub>2</sub>/bl-TiO<sub>2</sub>/FTO perovskite solar cell, suggesting the high charge collection during the illumination and results to the high electron-transport rate and the photocurrent density. Thus, the introduction of PANI-NPs as HTL might enhance the charge transfer time and the charge collection of the fabricated perovskite solar cells and produces the high performance of the perovskite solar cell.

#### 4. CONCLUSIONS

In summary, a unique and well-defined morphology of PANI-NPs as efficient HTL is employed to fabricate the high performance perovskite solar cell using methyl CH<sub>3</sub>NH<sub>3</sub>PbI<sub>3</sub> as sensitizer. The reasonable solar-to-electricity conversion efficiency of ~6.29 % with short circuit current ( $J_{SC}$ ) of ~17.97 mA/cm<sup>2</sup> and open circuit voltage ( $V_{OC}$ ) of ~0.877 V are obtained by Ag/PANI-NPs/CH<sub>3</sub>NH<sub>3</sub>PbI<sub>3</sub>/mp-anatase-TiO<sub>2</sub>/bl-TiO<sub>2</sub>/FTO perovskite solar cell. The IPCE measurement reveals that the fabricated Ag/PANI-NPs/CH<sub>3</sub>NH<sub>3</sub>PbI<sub>3</sub>/mp-anatase-TiO<sub>2</sub>/bl-TiO<sub>2</sub>/FTO perovskite solar cell presents the maximum value of ~51% in the wavelength range of ~450-700 nm and drops at longer wavelengths. The transient photocurrent and photovoltage studies elucidate that the fabricated solar cell exhibits a high  $\eta_{CC}$  value, suggesting the high charge collection during the illumination due to good transport time and the low recombination time which significantly results to high electron-transport rate and the photocurrent density. Hence, the use of PANI-NPs as HTL improves the charge carrier generation and the charge collection efficiency of the fabricated perovskite solar cell.

#### ACKNOWLEDGEMENTS

1  
2  
3 Dr. Sadia Ameen acknowledges the Research Funds of Chonbuk National University in  
4  
5 2012. This work is fully supported by NRF Project # 2014R1A2A2A01006525. This work is  
6  
7 also supported by “Leaders in Industry-University Cooperation Project”(2014), supported by the  
8  
9 Ministry of Education, Science & Technology (MEST) and the National Research Foundation of  
10  
11 Korea (NRF). We acknowledge the Korea Basic Science Institute, Jeonju branch, for utilizing the  
12  
13 research supported facilities.  
14  
15

16  
17 **Supporting Information**  
18

19 This material is available free of charge via the Internet at <http://pubs.acs.org>.  
20  
21  
22  
23

24  
25 **REFERENCES**  
26

- 27 (1) Mosconi, E.; Amat, A.; Nazeeruddin, M. K.; Grätzel, M.; De Angelis, F. Article First-  
28 Principles Modeling of Mixed Halide Organometal Perovskites for Photovoltaic Applications, *J.*  
29 *Phys. Chem. C* **2013**, *117*, 13902-13913.  
30  
31 (2) Liu, M.; Johnston, M.; Snaith, H., Efficient planar heterojunction perovskite solar cells by  
32 vapour deposition, *Nature* **2013**, *501*, 395-398.  
33  
34 (3) Kagan, C. R.; Mitzi, D. B.; Dimitrakopoulos, C. D., Organic-Inorganic Hybrid Materials as  
35 Semiconducting Channels in Thin-Film Field-Effect Transistors, *Science* **1999**, *286*, 945-947.  
36  
37 (4) Edri, E.; Kirmayer, S.; Cahen, D.; Hodes, G. High Open-Circuit Voltage Solar Cells Based  
38 on Organic-Inorganic Lead Bromide Perovskite *J. Phys. Chem. Lett.* **2013**, *4* (6), 897-902.  
39  
40 (5) Ball, J.; Lee, M.; Hey, A.; Snaith. H., Low-temperature processed meso-superstructured to  
41 thin-film perovskite solar cells. *Energy Environ. Sci.* **2013**, *6*, 1739-1743.  
42  
43  
44  
45  
46  
47  
48  
49  
50  
51  
52  
53  
54  
55  
56  
57  
58  
59  
60

- 1  
2  
3 (6) Lee, M. M.; Teuscher, J.; Miyasaka, T.; Murakami, T. N.; Snaith, H. J., Efficient Hybrid  
4 Solar Cells Based on Meso-Superstructured Organometal Halide Perovskites, *Science* **2012**, *338*,  
5  
6 643-647.  
7  
8 (7) Chung, I.; Lee, B.; He, J. Q.; Chang, R. P. H.; Kanatzidis, M. G., All-solid-state dye-  
9 sensitized solar cells with high efficiency, *Nature* **2012**, *485*, 486-494.  
10  
11 (8) Mitzi, D. B.; Synthesis, Structure, and Properties of Organic-Inorganic Perovskites and  
12 Related Materials. In *Prog. Inorg. Chem.* John Wiley & Sons, Inc.: New York, 2007; pp 1-121.  
13  
14 (9) Lee, H. J.; Leventis, H. C.; Haque, S. A.; Torres, T.; Gratzel, M.; Nazeeruddin, M. K.;  
15 Panchromatic response composed of hybrid visible-light absorbing polymers and near-IR  
16 absorbing dyes for nanocrystalline TiO<sub>2</sub>-based solid-state solar cells, *J. Power Sour.* **2011**, *196*,  
17  
18 596-599.  
19  
20 (10) Mor, G. K.; Kim, S.; Paulose, M.; Varghese, O. K.; Shankar, K.; Basham, J.; Grimes, C. A.  
21 Visible to Near-Infrared Light Harvesting in TiO<sub>2</sub> Nanotube Array-P3HT Based Heterojunction  
22  
23 Solar Cells, *Nano Lett.* **2009**, *9*, 4250-4257.  
24  
25 (11) Grancini, G.; Kumar, R. S. S.; Abrusci, A.; Yip, H. L.; Li, C. Z.; Jen, A. K. Y.; Lanzani, G.;  
26 Snaith, H. J.; Boosting Infrared Light Harvesting by Molecular Functionalization of Metal  
27 Oxide/Polymer Interfaces in Efficient Hybrid Solar Cells, *Adv. Funct. Mater.* **2012**, *22*, 2160-  
28  
29 2166.  
30  
31 (12) Abrusci, A.; Ding, I. K.; Al-Hashimi, M.; Segal-Peretz, T.; McGehee, M. D.; Heeney, M.;  
32 Frey, G. L.; Snaith, H. J.; Facile infiltration of semiconducting polymer into mesoporous  
33 electrodes for hybrid solar cells, *Energy Environ. Sci.* **2011**, *4*, 3051-3058.  
34  
35 (13) Heo, J. H.; Im, S. H.; Noh, J. H.; Mandal, T. N.; Lim, C. S.; Chang, J. A.; Lee, Y. H.; Kim,  
36 H. J.; Sarkar, A.; Nazeeruddin, M. K.; Gratzel, M.; Seok, S; Efficient inorganic-organic hybrid  
37  
38  
39  
40  
41  
42  
43  
44  
45  
46  
47  
48  
49  
50  
51  
52  
53  
54  
55  
56  
57  
58  
59  
60

1  
2  
3 heterojunction solar cells containing perovskite compound and polymeric hole conductors,  
4  
5 *Nature photonics* **2013**, *7*, 486-491.  
6  
7

8 (14) Ameen, S.; Akhtar M.S.; Kim, Y. S.; Yang, O-B.; Shin, H. S. Sulfamic Acid-Doped  
9 Polyaniline Nanofibers Thin Film-Based Counter Electrode: Application in Dye-Sensitized Solar  
10 Cells, *J. Phys. Chem. C* **2010**, *114*, 4760-4764.  
11  
12

13 (15) Seo, H. K.; Ameen, S.; Akhtar, M. S.; Shin, H. S; Structural, morphological and sensing  
14 properties of layered polyaniline nanosheets towards hazardous phenol chemical, *Talanta* **2013**,  
15 *104*, 219-227.  
16  
17

18 (16) Ameen, S.; Akhtar, M. S.; Ansari, S. G.; Yang, O. B.; Shin, H. S; Electrophoretically  
19 deposited polyaniline/ZnO nanoparticles for p-n heterostructure diodes, *Superlatt. Microstr.*  
20 **2009**, *46*, 872-880.  
21  
22

23 (17) Xiao, Y.; Han, G.; Chang, Y.; Zhou, H.; Li, M.; Li, Y., An all-solid-state perovskite-  
24 sensitized solar cell based on the dual function polyaniline as the sensitizer and p-type hole-  
25 transporting material. *J. Power Sour.* **2014**, *267*, 1-8.  
26  
27

28 (18) Im, J. H.; Lee, C. R.; Lee, J. W.; Park, S. W.; Park, N. G; 6.5% efficient perovskite  
29 quantum-dot-sensitized solar cell, *Nanoscale* **2011**, *3*, 4088-4093.  
30  
31

32 (19) Qiu, J.; Qiu, Y.; Yan, K.; Zhong, M.; Mu, C.; Yan, H.; Yang, S; All-solid-state hybrid solar  
33 cells based on a new organometal halide perovskite sensitizer and one-dimensional TiO<sub>2</sub>  
34 nanowire arrays, *Nanoscale* **2013**, *5*, 3245-3248.  
35  
36

37 (20) Baikie, T.; Fang, Y.; Kadro, J. M.; Schreyer, M.; Wei, F.; Mhaisalkar, S. G.; Gratzel, M.;  
38 White, T. J., Synthesis and crystal chemistry of the hybrid perovskite (CH<sub>3</sub>NH<sub>3</sub>)PbI<sub>3</sub> for solid-  
39 state sensitised solar cell applications *J. Mater. Chem. A* **2013**, *1*, 5628-5641.  
40  
41

- 1  
2  
3 (21) Kim, H. S.; Lee, C. R.; Im, J. H.; Lee, K. B.; Moehl, T.; Marchioro, A.; Moon, S. J.;  
4 Humphry-Baker, R.; Yum, J. H.; Moser, J. E.; Gratzel, M.; Park, N. G; Lead Iodide Perovskite  
5 Sensitized All-Solid-State Submicron Thin Film Mesoscopic Solar Cell with Efficiency  
6 Exceeding 9%, *Sci. Rep.* **2012**, *2*, 591-7.  
7  
8 (22) Abrusci, A.; Stranks S.D.; Docampo P.; Yip H.-L.; Jen A. K.-Y.; Snaith H. J.; High  
9 performance perovskite-polymer hybrid solar cells via electronic coupling with fullerene  
10 monolayers. *Nano Lett.* **2013**, *13*, 3124-3128.  
11  
12 (23) Ameen, S.; Akhtar, M. S.; Kim, G. S.; Kim, Y. S.; Yang, O. B.; Shin, H. S; Plasma-  
13 enhanced polymerized aniline/TiO<sub>2</sub> dye-sensitized solar cells, *J. Alloys Comp.* **2009**, *487*, 382-  
14 386.  
15  
16 (24) Etgar, L.; Gao, P.; Xue, Z.; Peng, Q.; Chandiran, A. K.; Liu, B.; Nazeeruddin, M. K.;  
17 Grätzel, M. Mesoscopic CH<sub>3</sub>NH<sub>3</sub>PbI<sub>3</sub>/TiO<sub>2</sub> Heterojunction Solar Cells, *J. Am. Chem. Soc.* **2012**,  
18 *134*, 17396-17399.  
19  
20 (25) Koh, T. M.; Fu, K.; Fang, Y.; Chen, S.; Sum, T. C.; Mathews, N.; Mhaisalkar, S. G.; Boix,  
21 P. P.; Baikie, T. Formamidinium-Containing Metal-Halide: An Alternative Material for Near-IR  
22 Absorption Perovskite Solar Cells *J. Phys. Chem. C* **2014**, *118* (30), 16458–16462.  
23  
24 (26) Ameen, S. Akhtar, M. S. Kim, G. S. Kim, Y. S. Yang, O. B. Shin, H. S. Plasma-enhanced  
25 polymerized aniline/TiO<sub>2</sub> dye-sensitized solar cells, *J. Alloys Comp.* **2009**, *487*, 382-386.  
26  
27 (27) Li, W.; Li, J.; Wang, L.; Niu, G.; Gao, R.; Qiu Y. Post modification of perovskite sensitized  
28 solar cells by aluminum oxide for enhanced performance. *J. Mater. Chem. A* **2013**, *1*, 11735-  
29 11740.  
30  
31  
32  
33  
34  
35  
36  
37  
38  
39  
40  
41  
42  
43  
44  
45  
46  
47  
48  
49  
50  
51  
52  
53  
54  
55  
56  
57  
58  
59  
60

1  
2  
3 (28) Zhu, K.; Neale, N. R.; Miedaner, A.; Frank, A. J. Enhanced Charge-Collection Efficiencies  
4 and Light Scattering in Dye-Sensitized Solar Cells Using Oriented TiO<sub>2</sub> Nanotubes Arrays, *Nano*  
5  
6 *Lett.* **2006**, *7*, 69-74.  
7  
8

9  
10 (29) Katoh, R.; Kasuya, M.; Kodate, S.; Furube, A.; Fuke, N.; Koide, N. Effects of 4-tert-  
11 Butylpyridine and Li Ions on Photoinduced Electron Injection Efficiency in Black-Dye-  
12 Sensitized Nanocrystalline TiO<sub>2</sub> Films, *J. Phys. Chem. C* **2009**, *113*, 20738-20744.  
13  
14  
15  
16  
17  
18  
19  
20  
21  
22  
23  
24  
25  
26  
27  
28  
29  
30  
31  
32  
33  
34  
35  
36  
37  
38  
39  
40  
41  
42  
43  
44  
45  
46  
47  
48  
49  
50  
51  
52  
53  
54  
55  
56  
57  
58  
59  
60

**Figure Captions**

**Figure 1.** Surface FESEM images of (a) mp-TiO<sub>2</sub>/bl-TiO<sub>2</sub>/FTO, (b) CH<sub>3</sub>NH<sub>3</sub>PbI<sub>3</sub>/mp-TiO<sub>2</sub>/bl-TiO<sub>2</sub>/FTO and (c) the cross section of Ag/PANI-NPs/CH<sub>3</sub>NH<sub>3</sub>PbI<sub>3</sub>/mp-TiO<sub>2</sub>/bl-TiO<sub>2</sub>/FTO thin film.

**Figure 2.** Topographic (a, c) and three dimensional (b, d) AFM images of synthesized PANI NPs and PANI-NPs/CH<sub>3</sub>NH<sub>3</sub>PbI<sub>3</sub>/mp-TiO<sub>2</sub>/bl-TiO<sub>2</sub> thin film.

**Figure 3.** Elemental mapping (a) and the line scanning profile (b) of PANI-NPs/CH<sub>3</sub>NH<sub>3</sub>PbI<sub>3</sub>/mp-TiO<sub>2</sub>/bl-TiO<sub>2</sub> thin film.

**Figure 4.** XRD patterns of (a) CH<sub>3</sub>NH<sub>3</sub>PbI<sub>3</sub>/FTO and (b) CH<sub>3</sub>NH<sub>3</sub>PbI<sub>3</sub>/mp-TiO<sub>2</sub>/bl-TiO<sub>2</sub>/FTO thin films.

**Figure 5.** (a) UV-Vis spectra and (b) room temperature photoluminescence spectra of CH<sub>3</sub>NH<sub>3</sub>PbI<sub>3</sub>/FTO and PANI-NPs/CH<sub>3</sub>NH<sub>3</sub>PbI<sub>3</sub>/FTO thin film. Inset shows the UV-Vis spectrum of PANI NPs.

**Figure 6.** A schematic representation (a) and energy level diagram (b) of Ag/PANI-NPs/CH<sub>3</sub>NH<sub>3</sub>PbI<sub>3</sub>/FTO perovskite solar cell.

**Figure 7.** J-V curves (a) and Nyquist plots (b) of fabricated perovskite solar cells with and without PANI-NPs and (c) IPCE curve of the fabricated Ag/PANI-NPs/CH<sub>3</sub>NH<sub>3</sub>PbI<sub>3</sub>/FTO perovskite solar cell.

**Figure 8.** (a) IMVS and (b) IMPS measurement plots of the fabricated Ag/PANI/CH<sub>3</sub>NH<sub>3</sub>PbI<sub>3</sub>/FTO perovskite solar cell.

**Figure 9.** The electron transport (a) and the recombination lifetime of electrons (b) of the fabricated Ag/PANI-NPs/CH<sub>3</sub>NH<sub>3</sub>PbI<sub>3</sub>/FTO perovskite solar cell with respect to different incident photon fluxes.

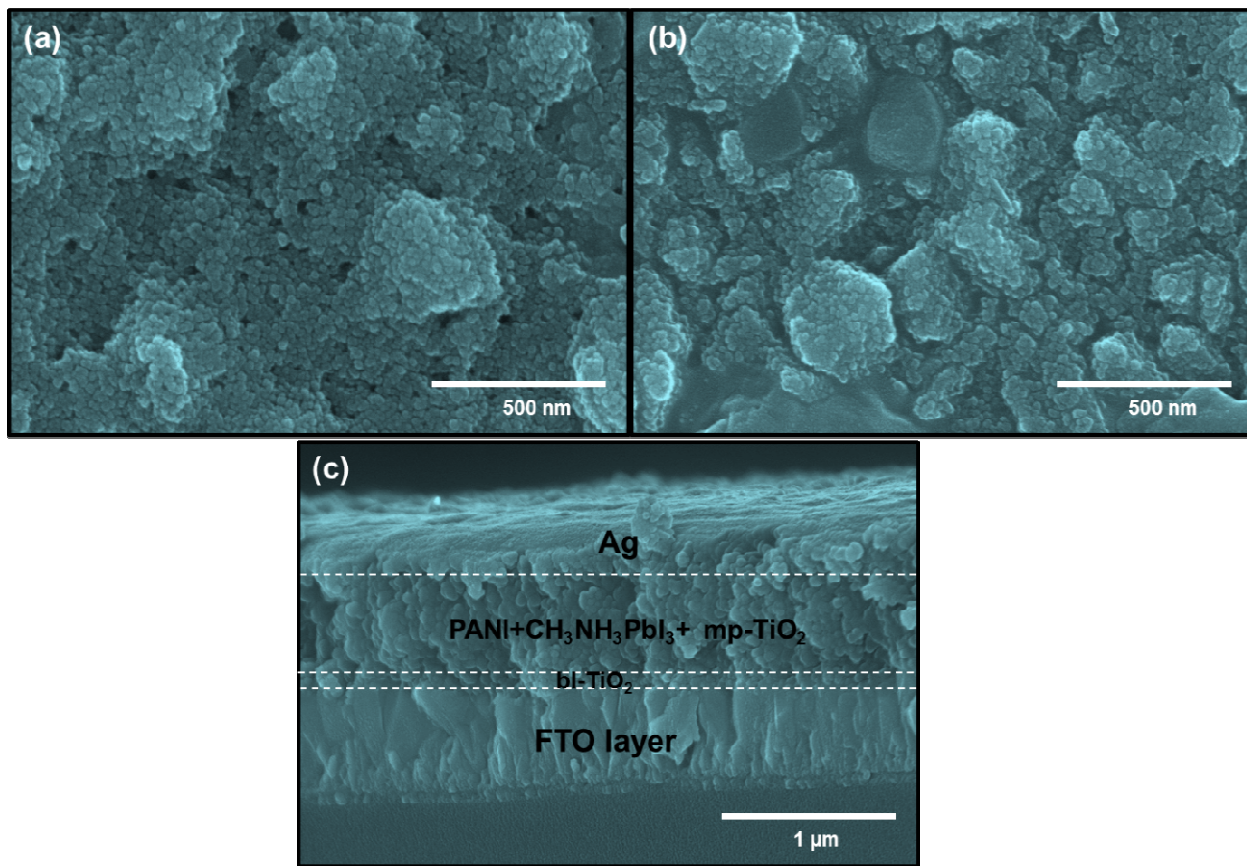


Figure 1

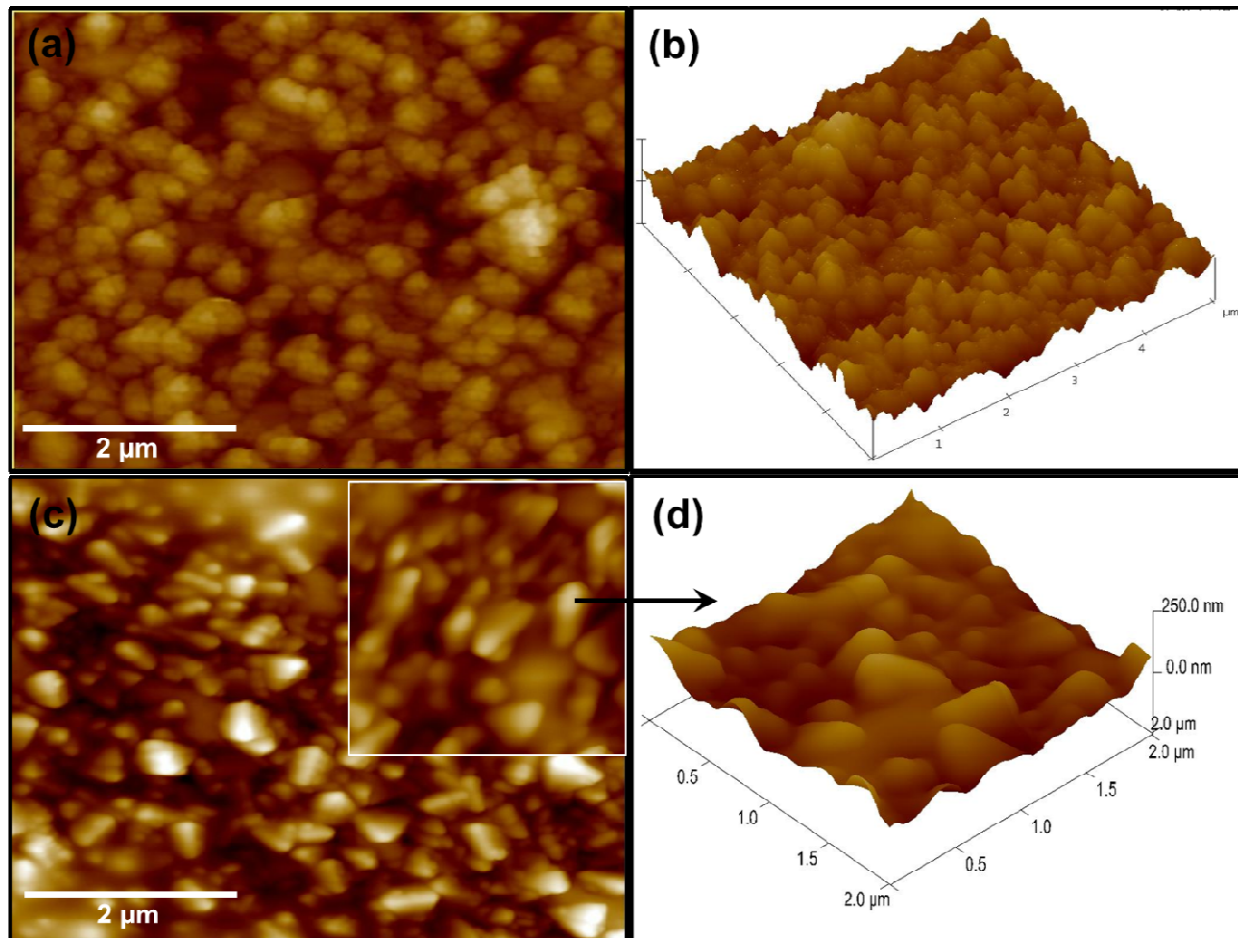


Figure 2

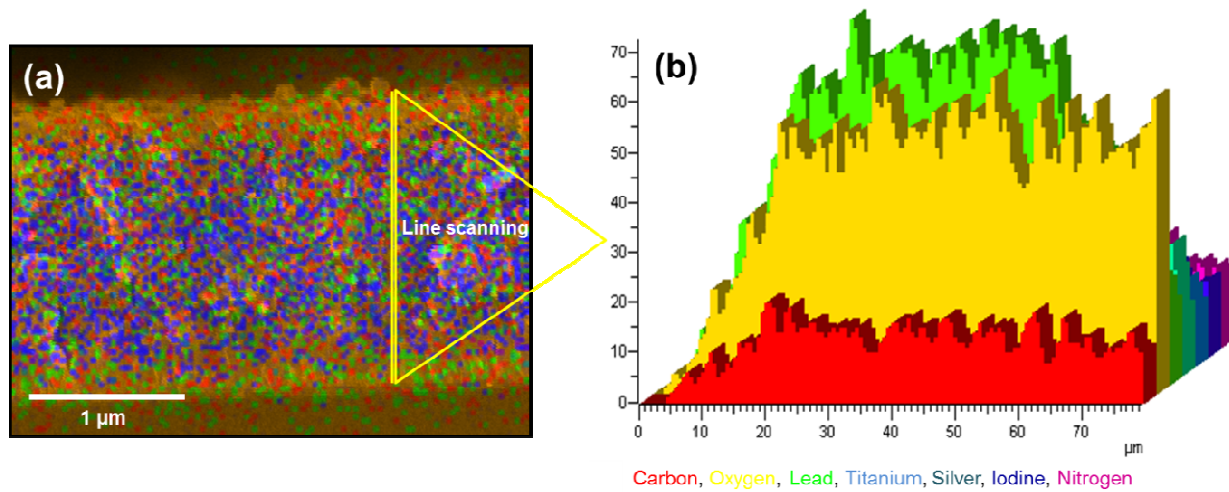


Figure 3

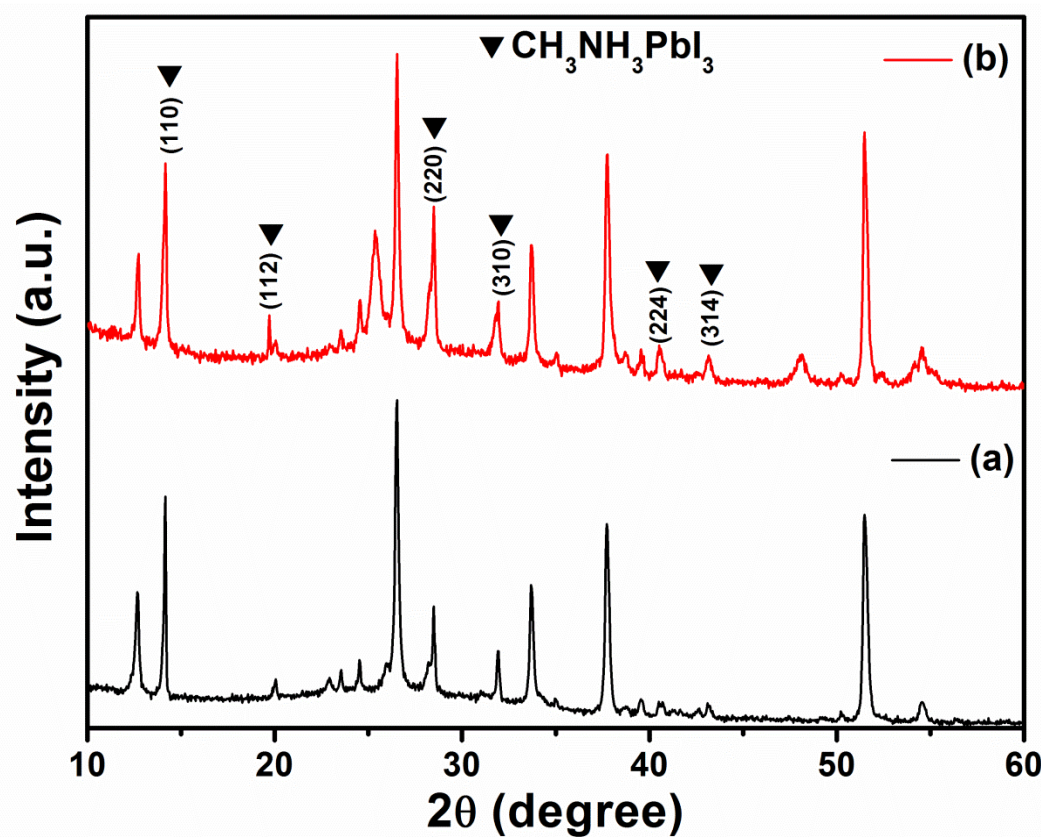


Figure 4

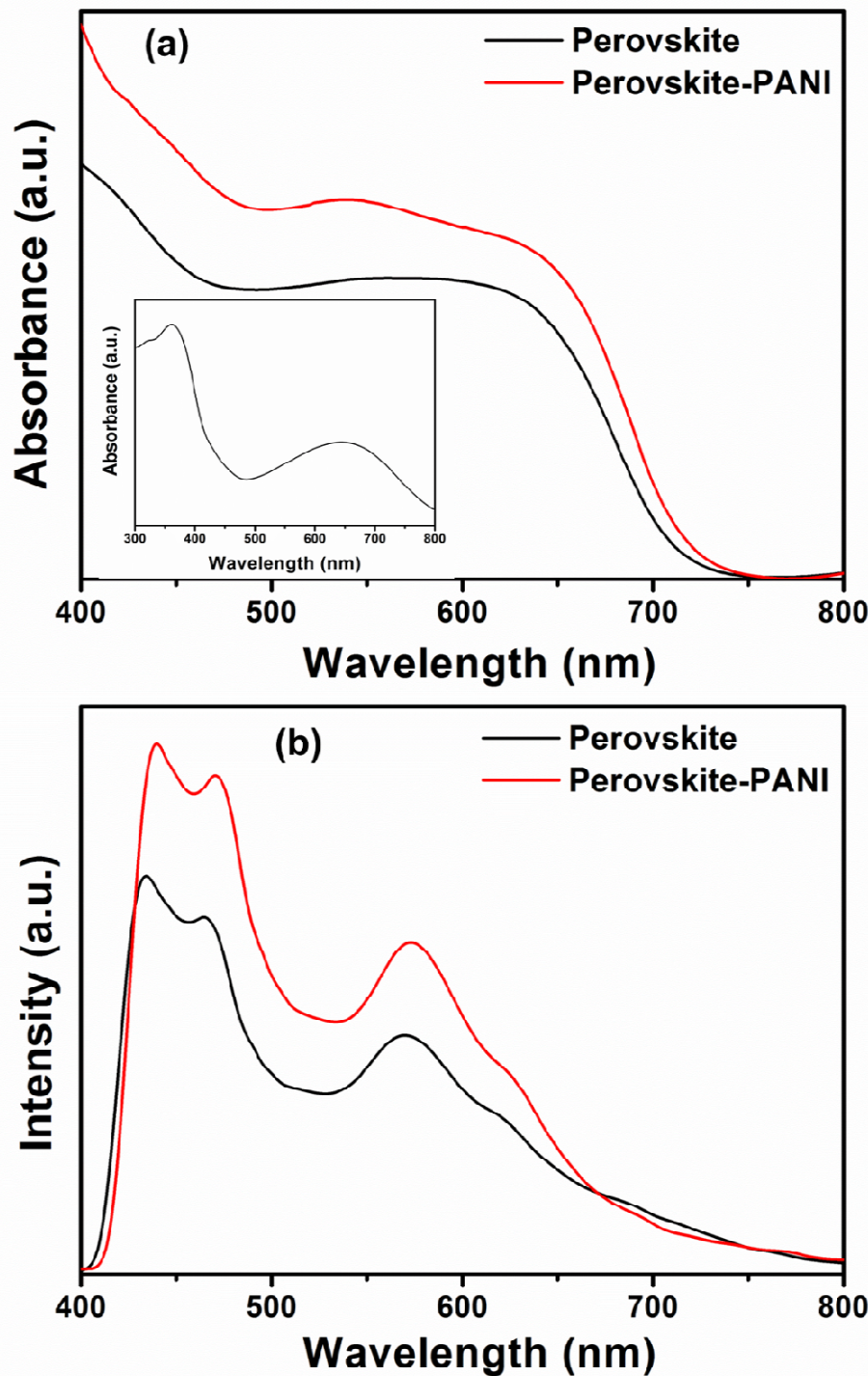


Figure 5

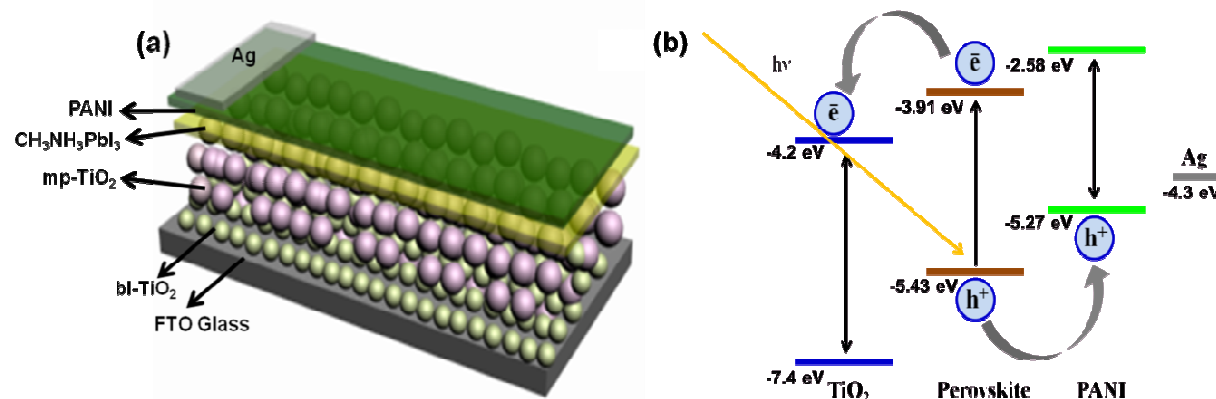


Figure 6

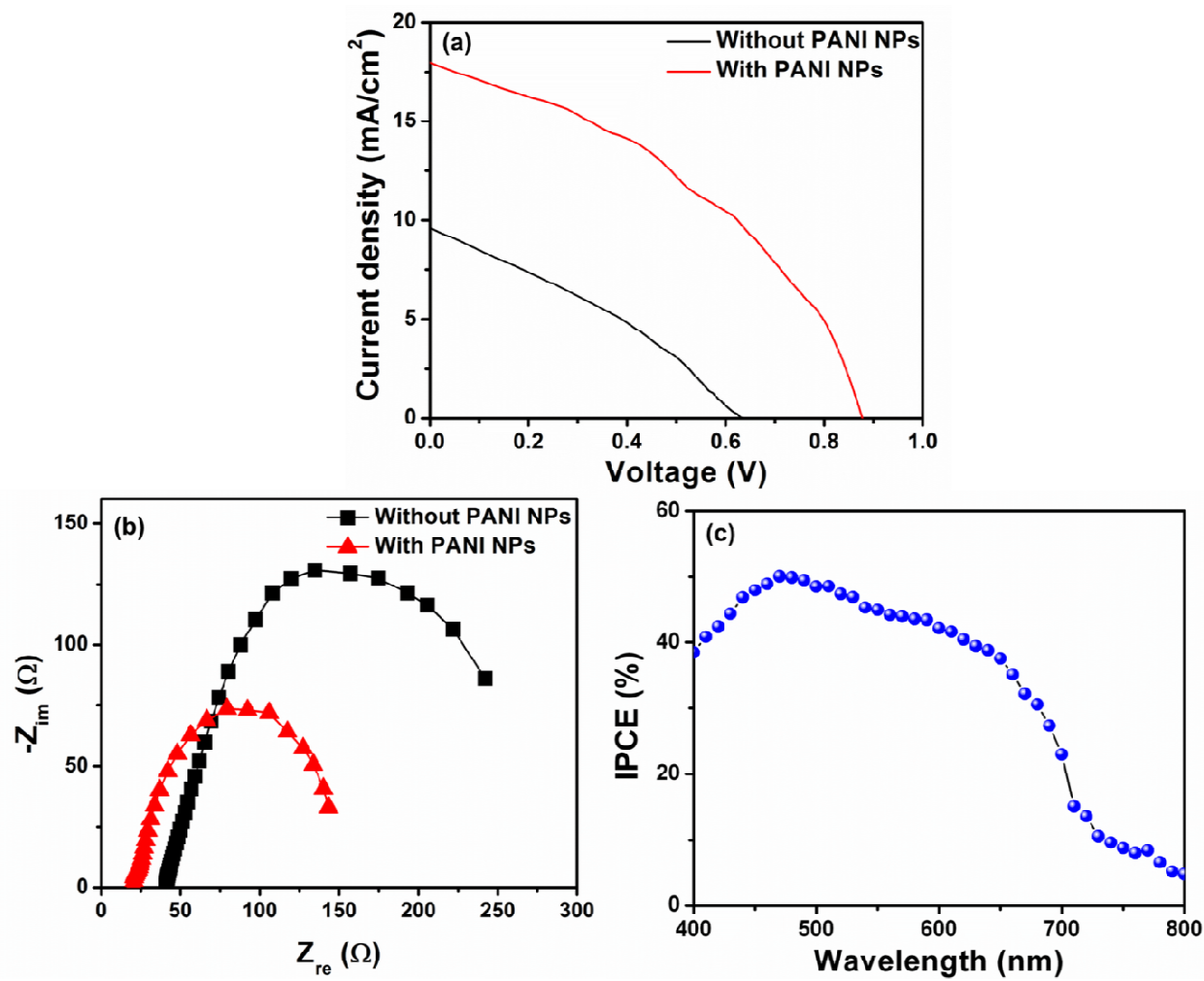


Figure 7

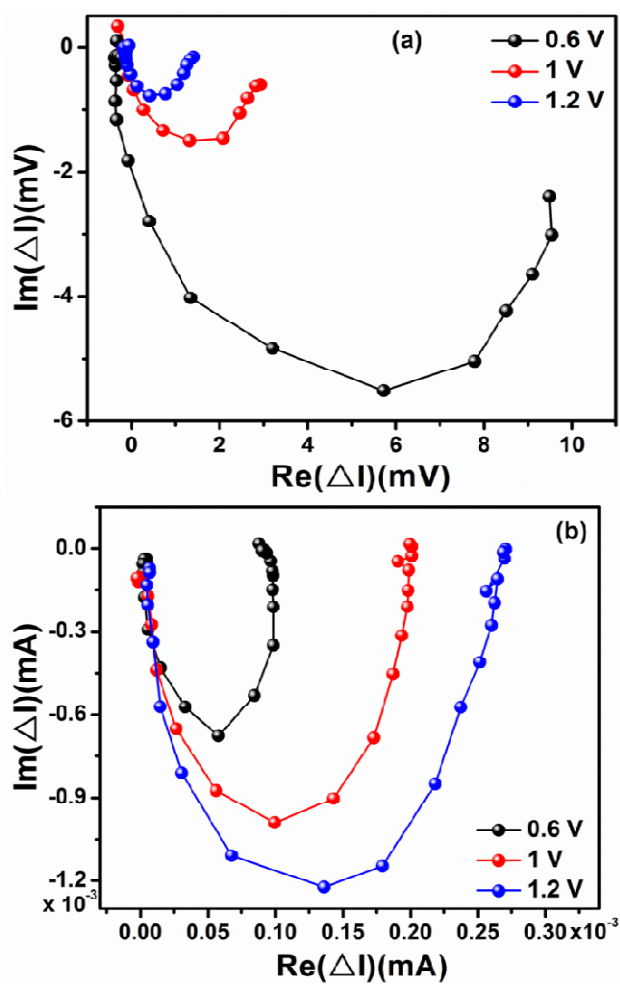


Figure 8

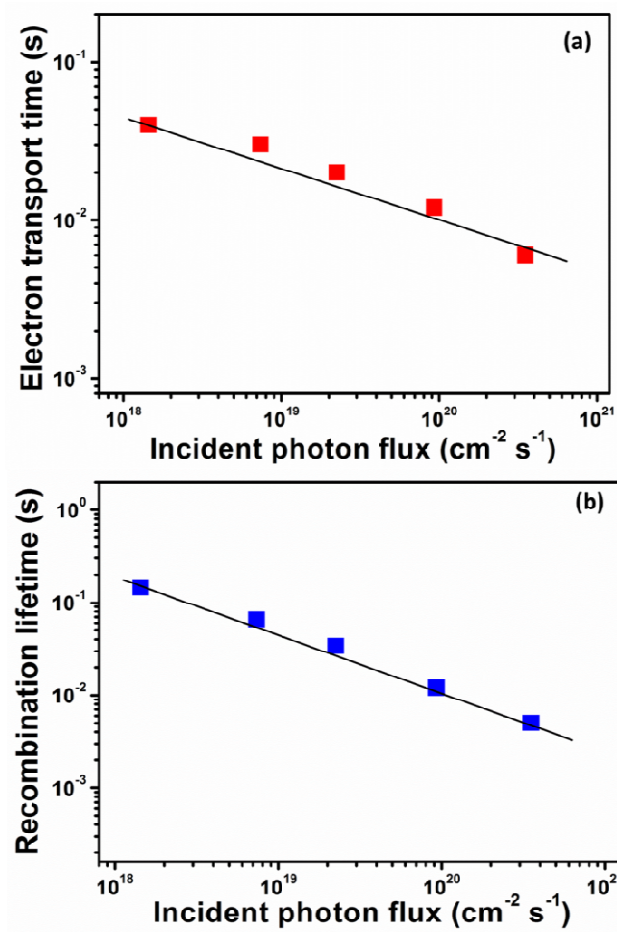


Figure 9

## Graphic

